



26 Traversing (CST) electrical surveys are very commonly undertaken for archaeological (see  
27 Gaffney 2008; Gaffney et al. 2015) and forensic (Juerges et al. 2010) targets, rapidly  
28 covering a survey area, albeit at very shallow depths. In contrast, Electrical Resistivity  
29 Tomography (ERT) surveys are relatively slower to collect but can penetrate up to 150 m  
30 below ground level (see Keary et al. 2002; Zhu et al. 2017).

31 Researchers can use a variety of different ERT electrode configurations (termed  
32 arrays - see Szalai and Szarka 2008); Reynolds (2011) provides theoretical background for  
33 the different array types. Published case study examples include using pole-pole arrays to  
34 detect underground cavities (Garman and Purcell 2004), using pole-dipole arrays to  
35 characterise Karst bedrock (Nyquist and Roth 2005), Saad et al. (2010) used Wenner,  
36 Wenner-Schlumberger and pole-dipole arrays to detect voids, Banham and Pringle (2011)  
37 used Wenner arrays to detect coal mineshafts, Cuthbert et al. (2009) used Wenner array to  
38 study the superficial deposits architecture effects on groundwater recharge, and finally  
39 Cardarelli et al. (2010) used pole-dipole arrays to detect buried cavities.

40 Most ERT surveys in brownfield sites use 2D survey array configurations, due to their  
41 relatively rapid deployment and data collection speeds, usually after other geophysical  
42 surveys have approximately located target(s) positions (Reynolds 2011). Best practice  
43 (Reynolds 2011) suggests that the buried target occurs along the plane of the survey line and  
44 in a perpendicular direction as others have suggested (Bentley and Gharibi 2004; Loke 2015).  
45 3D ERT arrays are more time consuming to acquire, but produce more relevant results as  
46 resistivity variations will be in three dimensions. Resistivity data processing is also important,  
47 the collected data should be checked for consistency and quality, and routinely inverted by  
48 specialist software programmes to convert collected apparent to interpreted resistivity values  
49 (see Loke & Barker 1996; Loke & Dahlin 2002; Loke et al. 2003, 2007, 2010).

50 Several array comparisons studies have already been published. For example,  
51 Kampke (1999) compared the inversion process for linear arrays (Wenner alpha) for  
52 archaeological prospecting, and found that the focused imaging method could produce a good  
53 estimation of subsurface anomalies. Dahlin and Zhou (2004) compared several different array  
54 configurations on five synthetic datasets with anomalies present, using a least-square  
55 smoothness-constraint and robust inversions, and Stummer et al. (2004), Maurer et al. (2010)  
56 and Wilkinson et al. (2006/2012) compared optimised ERT survey designs. Results showed  
57 that pole-dipole, dipole-dipole, multiple gradient and Schlumberger arrays were  
58 recommended for 2D resistivity surveys, with array choice related to the geology, logistic  
59 issues and other site-specific variables.

60 For civil engineering purposes, resistivity surveys have been used to detect and  
61 characterise sites, for example, to determine subsurface characterization (Soupios et al. 2007),  
62 investigation of existing foundations (e.g. Cardarelli et al. 2007; Arjwech et al. 2013), or to  
63 monitor ground stabilisation procedures (e.g. Fischanger et al. 2013; Apuani et al. 2015).  
64 Resistivity imaging has been used for railway embankment conditions assessment (Donohue  
65 et al. 2011; Gunn et al. 2015). Moreover, ERT has been used for detecting natural (Deceuster  
66 et al., 2006; Zhu et al., 2011) and man-made (Chambers et al. 2007; Cardarelli et al. 2010;  
67 Orfanos and Apostolopoulos 2011) underground cavities as possible hazards that might be  
68 effect civil construction integrity. Cardarelli et al. (2018) undertook 3D ERT surveys, as well  
69 as seismic tomographic surveys, to assess the conditions of an ancient Roman historical  
70 building. However, there has been little research to assess preferable 2D profile array  
71 configurations for detection and characterisation of cleared-wall foundations in brownfield  
72 sites.

73 More-sophisticated ERT interpretation methods use data inversion as a tool, to  
74 produce a 2D section of implied resistivity values from measured apparent resistivity data.

75 The main aim of inversion theory is to produce an interpreted resistivity model of the sub-  
76 surface, that provides simulated apparent resistivity values that are a best match/fit to the  
77 collected data (see Loke and Barker 1995). The forward modelling programme generates  
78 simulated data, based on a finite-difference or finite-element method, and then the inversion  
79 technique is used to iteratively change the model until the simulated data matches the  
80 collected data (Dahlin 2001). The difference between simulated and collected data is  
81 measured and presented as root mean square (RMS) errors (see Loke and Dahlin 2002).

82 This paper aims to evaluate surface 2D ERT surveys to detect cleared-wall  
83 foundations in brownfield sites, and their appropriate survey parameters. Study objectives  
84 will therefore be to: (1) collect multiple 2D ERT datasets over a scaled model of a cleared-  
85 wall foundation in gravel-fill on a test site; (2) repeat the surveys using the four most  
86 commonly-used ERT array configurations (Wenner, dipole-dipole, pole-dipole, and pole-  
87 pole); (3) invert all datasets with the two commonly-used least-squares and robust methods  
88 and finally; (5) determine the best array type and inversion methods for 2D datasets.

**89 The test facility site**

90 The test site lies within the grounds of Keele University in Staffordshire, United Kingdom.  
91 The bedrock geology is the late Carboniferous clastic sedimentary Butterton Sandstone Bed  
92 of the Halesowen Formation at 1.2 m below ground level (bgl), with overlying Quaternary  
93 glacial sandy soil deposits and water table depth at 3 m - 4 m bgl (Cassidy 2001).

94 A test pit, 0.8 m deep, 3 m long and 2.9 m wide, was excavated and a central  
95 Victorian brick wall foundation built, 1.5 m long, 0.36 m wide and 0.48 m high, orientated in  
96 an East-West direction (Fig. 1). The excavated sides were covered by an impermeable  
97 membrane and drainage added before the wall was built. The pit was then back-filled with  
98 clay-free, well-sorted, 4 mm quartz gravel and, with porosity of about 42%, to a depth of  
99 ~0.55 m. The final ~0.25 m was refilled by re-cycled, compacted top soil and the test site  
100 levelled (Cassidy 2001).

101 Fig. 1

102

**103 Survey methodology and data processing**

104 Two sets of ERT surveys were collected across the test site, over a period of 15 days,  
105 orientated north-south and east-west respectively (Fig. 2). Each survey consisted of three  
106 parallel 2D ERT profiles of 64 electrodes with 0.25 m electrode spacing (Fig. 2). The 16 m  
107 long ERT profile lengths were determined to gain sufficient penetration in the target area  
108 following initial trials. Repeat Wenner, pole-pole, dipole-dipole, and pole-dipole array ERT  
109 configurations (as well as repeats in both directions) were collected at each profile position  
110 (see Reynolds 2011 ch. 7 for more information).

111 In this study, the CAMPUS™ Tigre resistivity meter was used for data collection,  
112 using Imager™ pro 2006 v.1.1.4 controller software. Once the electrode probe contact

113 resistances were checked for consistency for each profile, the meter was set to collect each  
114 reading with a 1 s duration and 3 cycles to gain an average. The number of resistivity data  
115 points and investigated resistivity levels were kept the same for each profile array for  
116 consistency purposes.

117         Within the N-S orientated ERT survey set, profile NS1 was located over the wall  
118 foundation centre, profile NS2 was located 0.75 m to the east of the foundation (at the wall-  
119 gravel interface) and profile NS3 was located 2.5 m to the east of the foundation (Fig. 2).  
120 Within the E-W orientated survey set, profile EW1 was located over the wall foundation  
121 centre, profiles EW2 and EW3 were located 0.75 m and 4 m to the north of the foundation  
122 respectively (Fig. 2).

123

124 Fig.2

125

126         The resulting ERT datasets were initially checked for consistency and quality, with  
127 anomalous data points (compared to adjacent measurements but considering target locations)  
128 removed and adjacent measurements utilised to give an average value for removed points  
129 using Surfer™ v.8.04 software. The number of collected and corrected data points are detailed  
130 in Table 1. All resistivity surveys investigated deeper than the bottom of the cleared-wall  
131 foundation, but the pole-pole data sets had a significant number of zero readings recorded,  
132 therefore, just the target section was selected and processed to generate 2D resistivity models.  
133 Note that the pole-dipole array configuration collects asymmetrical data (see Loke 2015), so  
134 these data were collected on each survey profile in both directions, and the resulting pole-  
135 dipole data merged to produce the respective images (Figs 3-4).

136

137

138 Table 1

139           Respective ERT array datasets were then finite-difference inverted within Geotomo™  
140 Res2Dinv v.3.4 software, using first the non-linear, least-squares optimization algorithm  
141 (using normal mesh and damping factors), and secondly using the robust inversion algorithms  
142 (using respective 0.05 data and 0.01 model constrain cutoffs) for comparison (see Loke &  
143 Barker 1996; Loke et al. 2007). The 5<sup>th</sup> model iteration and a common logarithmic, colour-  
144 contoured interval was used throughout for consistency. The software set the depth of 'n'  
145 level 1 at ~0.5 electrode spacing (a) for the Wenner, ~0.3a for dipole-dipole, 0.6a for pole-  
146 dipole and 0.9a for pole-pole array configurations respectively based on Edwards (1977).  
147

148 **Results**

149           The 2D resistivity models (Figs. 3-6) showed obvious apparent resistivity contrasts  
150 between the test site gravel-fill materials and the natural ground, these materials having  
151 relatively high resistivity values (~2000 ohm.m or more) comparing to the background  
152 natural ground soil (~100-500 ohm.m). The brick wall foundation, compared to the gravel-fill  
153 volume, was less easily resolved in the 2D resistivity models (marked in Figs. 3-6), having  
154 relatively higher resistivity values (~3000 ohm.m or more), compared to the gravel-fill  
155 material. Based on the resistivity contrast between the natural background, the gravel-fill, the  
156 brick wall foundation, and the test site's dimensions (see Fig. 1), the resistivity models were  
157 then interpreted and compared.

158           The test site with gravel-fill material (annotated by the dotted white boxes on the 2D  
159 resistivity models – Figs. 3-6), had its spatial extent generally well imaged by all four array  
160 types, with the Wenner array better defining the test site edges and the dipole-dipole array  
161 better at defining the test site depth (Figs 3-4). The dipole-dipole and pole-dipole arrays were  
162 generally better at imaging the top of the buried wall foundation, whilst the Wenner and pole-  
163 pole arrays were better at imaging the bottom of the foundation (Figs 3-6); comparing with  
164 foundation's dimensions and position (*cf.* Figs. 3-6).

165           The thin top soil, of relatively lower resistivity, compared to the rest of the site, was  
166 well constrained and equally well defined in all array configurations.

167           Based on the comparing the different electrode configurations, these 2D resistivity  
168 models were then qualitatively assessed based on two parameters: 1) the successful imaging  
169 of the cleared-brick wall foundation (i.e. which array could detect and discriminate the  
170 foundation from the gravel-fill) and, 2) the cleared-brick wall foundation accurate positioning  
171 (i.e. to what extent the brick wall position could be accurately located by the different array  
172 types). The assessment was ranked *Good* when the resistivity model (i.e. of a certain



173 electrode configuration) achieved the two assessment parameters, *Moderate* when the model  
174 achieved one and ranked *Poor* when the model did not achieve either parameter. These were  
175 calculated for both the least-squares and robust inversion methods. Summary of these results  
176 are detailed in Table 2.

177 For the least-squares inverted data profiles (Figs 3-4), the Wenner and dipole-dipole  
178 arrays generally gave *Good* results, whilst the pole-dipole and pole-pole array generally gave  
179 *Moderate* to *Poor* results (Table 2). Note that the wall foundation appeared to be spatially  
180 wider on EW profiles, when compared to the NS profiles (cf. Figs 3-4), as the EW profiles  
181 were orientated parallel to the buried target (Fig. 2).

182 For the robust inverted data profiles (Figs 5-6), the Wenner and dipole-dipole arrays  
183 generally gave *Moderate* results, whilst the pole-dipole and pole-pole arrays generally gave  
184 *Poor* results (Table 2). With these inversions, it was also harder to differentiate the cleared-  
185 brick wall foundation from the gravel-fill materials (cf. Fig. 5-6).

186

187 **Discussion**

188           This study has therefore investigated using electrical resistivity surveys to image a  
189 scaled model of a cleared-brick wall foundation, a common target for geotechnical  
190 geophysical surveys, especially in brownfield development sites (see Reynolds 2011). 2D  
191 ERT datasets were collected using the Wenner, dipole-dipole, pole-dipole and pole-pole array  
192 types, with data subsequently separately inverted during data processing using both least-  
193 squares and robust inversion algorithms. The resulting datasets found that the Wenner and  
194 dipole-dipole arrays generally located the position of the cleared-brick wall foundation,  
195 although not its base. The dipole-dipole configuration was more accurate, overall, than the  
196 Wenner for size/dimension of the target, which is surprising as most site investigations use  
197 the Wenner array (e.g. see Saad et al. 2010; Banham & Pringle 2011). The pole-pole array  
198 was generally the poorest in terms of target location and image quality.

199           The orientation of the 2D ERT profiles, in regards to the target location, was also  
200 found to be important, whilst all four arrays could detect the target in profiles parallel rather  
201 than only two detecting it in profiles perpendicular to the target, presumably as it was a larger  
202 target (1.5 m compared to 0.36 m respectively). Therefore, if the target orientation was not  
203 known in a site survey, multiple orientations of ERT 2D profiles should be collected to  
204 optimise survey results.

205           The study also illustrated the importance of minimum electrode spacing with regard to  
206 the target dimensions. Although the electrode spacing was a constant 0.25 m throughout all  
207 collected ERT survey profiles, the type of array significantly affected the respective survey  
208 array sensitivities. For example, the pole-pole array had a  $\sim 0.5x$  electrode spacing = 0.5 m  
209 minimum target size, the pole-dipole array had a  $\sim 1.6x$  electrode spacing = 0.4 m minimum  
210 target size, the dipole-dipole array had a  $\sim 1.8x$  electrode spacing = 0.45 m minimum target  
211 size and lastly the Wenner array had a  $\sim 1.7x$  electrode spacing = 0.425 m minimum target

212 size respectively – see Loke 2015). Thus this study finds that the array type is just as, if not  
213 more important than the electrode spacing to be optimal when designing electrical resistivity  
214 arrays. 2D ERT profiles will be sufficient to define a target where its approximate position is  
215 known, as Lysdahl et al. 2017 showed on coastal harbour foundations.

216 It would be preferable to quantify target anomaly contrasts with background materials,  
217 as others have undertaken in seismic surveys (see, for example, Guerriero et al. 2016; 2017).

218 Study limitations included the constrained nature of the test site surroundings (similar  
219 to those expected in urban brownfield sites) which limited survey profile lengths, and the  
220 strong contrast between the non-target gravel-fill and the background soils, which made it  
221 more difficult to resolve the target brick wall foundation. 3D surveys may have allowed  
222 unusual survey configurations to be collected, as Tejero-Andrade et al. (2015) illustrate, but  
223 this is unusual in commercial investigations of brownfield sites due to the extra time and  
224 associated costs incurred. Further work should collect 3D datasets, and vary the water content  
225 percentages in the surrounding pit to determine what effect these variations will have on  
226 target discrimination. Synthetic datasets could also be generated, varying the target body  
227 dimensions, depths below ground levels and other soil types to test these major variables.

228

229 **Conclusions**

230 Multiple ERT 2D profiles were collected over a controlled study site with a scaled  
231 model of a cleared-brick wall foundation, emplaced within a gravel-filled test site with a thin  
232 top soil. Wenner, dipole-dipole, pole-dipole and pole-pole configurations were trialled, before  
233 being separately inverted using both least-squares and robust inversion types. For the 2D  
234 resistivity surveys, the Wenner and dipole-dipole produced the best results, imaging the brick  
235 wall foundation, but not its base. Array type was deemed just as, or even more important than,  
236 electrode spacing when designing electrical resistivity surveys, due to different array type  
237 sensitivities to buried targets.

238

239

240 **Acknowledgments**

241           The Higher Committee for Education Development in Iraq (HCED) have provided  
242 funding for Raad Eissa's PhD. A 2003 SRIF2 UK Research Council award supported the  
243 geophysical equipment used during this research. EDINA Digimap is acknowledged for data  
244 retrieval support. Two anonymous reviewers greatly improved the manuscript for which the  
245 authors are grateful.

246

247

248 **References**

249 al Hagrey, S. A. and Petersen, T. 2011. Numerical and experimental mapping of small root  
250 zones using optimized surface and borehole resistivity tomography. *Geophysics*, **76**, G25-  
251 G35, <https://dx.doi.org/10.1190/1.3545067>.

252 Apuani, T, Giani, G.P., d'Attoli, M., Fischanger, F., Morelli, G., Ranieri, G., and Santarato,  
253 G. 2015. Assessment of the efficiency of consolidation treatment through injections of  
254 expanding resins by geotechnical tests and 3D electrical resistivity tomography. *The*  
255 *Scientific World Journal*, article ID 237930, 1-13, <https://dx.doi.org/10.1155/2015/237930>.

256 Arjwech, R., Everett, M.E., Briaud, J.L., Hurlebaus, S., Medina-Cetina, Z., Truker, S. and  
257 Yousefpour, N. 2013. Electrical resistivity imaging of unknown bridge foundations. *Near*  
258 *Surface Geophysics*, **11**, 591-598, <https://dx.doi.org/10.3997/1873-0604.2013023>.

259 Banham, S.G. and Pringle, J.K. 2011. Geophysical and intrusive site investigations to detect  
260 an abandoned coal-mine access shaft, Apedale, Staffordshire, UK. *Near Surface*  
261 *Geophysics*, **9**, 483-496, <https://dx.doi.org/10.3997/1873-0604.2011028>.

262 Bentley, L.R. and Gharibi, M. 2004. Two- and three-dimensional electrical resistivity  
263 imaging at a heterogeneous remediation site. *Geophysics*, **69**, 674–680,  
264 <https://dx.doi.org/10.1190/1.1759453>.

265 Cardarelli, E., Donno, G., Oliveti, I. and Scatigno, C. 2018. Three-dimensional reconstruction  
266 of a masonry building through electrical and seismic tomography validated by biological  
267 analyses. *Near Surface Geophysics*, **16**, 53-65, [https://dx.doi.org/10.3997/1873-](https://dx.doi.org/10.3997/1873-0604.2017040)  
268 [0604.2017040](https://dx.doi.org/10.3997/1873-0604.2017040).

- 269 Cardarelli, E., Cercato, M., Cerreto, A. and Di Filippo, G. 2010. Electrical resistivity and  
270 seismic refraction tomography to detect buried cavities. *Geophysical Prospecting*, **58**, 685-  
271 695, <https://dx.doi.org/10.1111/j.1365-2478.2009.00854.x>.
- 272 Cardarelli, E., Cercato, M. and Di Filippo, G. 2007. Assessing foundation stability and soil-  
273 structure interaction through integrated geophysical techniques: a case history in Rome  
274 (Italy). *Near Surface Geophysics*, **5**, 141–147, [https://dx.doi.org/10.3997/1873-](https://dx.doi.org/10.3997/1873-0604.2006026)  
275 [0604.2006026](https://dx.doi.org/10.3997/1873-0604.2006026)
- 276 Cassidy, N. 2001. *The application of mathematical modelling in the interpretation of near-*  
277 *surface archaeological ground-penetration radar*. Ph.D. thesis, Keele University.
- 278 Chambers, J.E., Wilkinson, P.B., Weller, A.L., Meldrum, P.I., Ogilvy, R.D. and Caunt, S.  
279 2007. Mineshaft imaging using surface and crosshole 3D electrical resistivity tomography:  
280 A case study history from the East Pennine Coalfield, UK. *Journal of Applied Geophysics*,  
281 **62**, 324-337, <https://dx.doi.org/10.1016/j.jappgeo.2007.03.004>.
- 282 Chrétien, M., Lataste, J.F., Fabre, R. and Denis, A. 2014. Electrical resistivity tomography to  
283 understand clay behaviour during seasonal water content variations. *Engineering Geology*,  
284 **169**, 112-123, <https://dx.doi.org/10.1016/j.enggeo.2013.11.019>.
- 285 Cosenza, P., Marmet, E., Rejiba, F., Cui, Y., Tabbagh, A. and Charlery, Y. 2006.  
286 Correlations between geotechnical and electrical data: a case study at Garchy in France.  
287 *Journal of Applied Geophysics*, **60**, 165–178,  
288 <https://dx.doi.org/10.1016/j.jappgeo.2006.02.003>.
- 289 Dahlin, T. 2001. The development of DC resistivity imaging techniques. *Computers &*  
290 *Geosciences*, **27**, 1019-1029, [https://dx.doi.org/10.1016/S0098-3004\(00\)00160-6](https://dx.doi.org/10.1016/S0098-3004(00)00160-6).

291 Dahlin, T. and Zhou, B. 2004. A numerical comparison of 2D resistivity imaging with 10  
292 electrode arrays. *Geophysical prospecting*, **52**, 379-398,  
293 <https://dx.doi.org/10.1111/j.1365-2478.2004.00423.x>.

294 Deceuster, J., Delgranche, J., Kaufmann, O. and 2006. 2D cross-borehole resistivity  
295 tomographies below foundations as a tool to design proper remedial actions in covered  
296 karst. *Journal of Applied Geophysics*, **60** (1), 68–86,  
297 <https://dx.doi.org/10.1016/j.jappgeo.2005.12.005>.

298 Donohue, S., Gavin, K. and Tolooiyan, A. 2011. Geophysical and geotechnical assessment of  
299 a railway embankment failure. *Near Surface Geophysics*, **9** (1), 33–44,  
300 <https://dx.doi.org/10.3997/1873-0604.2010040>.

301 Edwards, L.S. 1977. A modified pseudosection for resistivity and induced-polarization.  
302 *Geophysics*, **42** (5), 1020-1036, <https://dx.doi.org/10.1190/1.1440762>.

303 Fischanger, F., Morelli, G., Ranieri, G., Santarato, G., and Occhi, M. 2013. 4D cross-  
304 borehole electrical resistivity tomography to control resin injection for ground stabilization:  
305 a case study history in Venice (Italy). *Near Surface Geophysics*, (11), 41-50,  
306 <https://dx.doi.org/10.3997/1873-0604.2012056>.

307 Gaffney, C., Harris, C., Pope-Carter, F., Bonsall, J., Fry, R. And Parkyn, A. 2015. Still  
308 searching for graves: an analytical strategy for interpreting geophysical data used in the  
309 search for “unmarked” graves. *Near Surface Geophysics*, **13**, 557-569,  
310 <https://dx.doi.org/10.3997/1873-0604.2015029>.

311 Gaffney, C. 2008. Detecting trend in the prediction of the buried past: a review of  
312 geophysical techniques in archaeology. *Archaeometry*, **50**, 313-336,  
313 <https://dx.doi.org/10.1111/j.1475-4754.2008.00388.x>.



- 314 Garman, K. and Purcell, S. 2004. Three-dimensional electrical resistivity surveys to identify  
315 buried karst features affecting road projects, subsurface evaluation, Inc. [Available  
316 online]:[http://www.dot.state.fl.us/statematerialsoffice/geotechnical/conference/materials//g](http://www.dot.state.fl.us/statematerialsoffice/geotechnical/conference/materials//garman-pursel.pdf)  
317 [arman-pursel.pdf](http://www.dot.state.fl.us/statematerialsoffice/geotechnical/conference/materials//garman-pursel.pdf). [Accessed 09/02/2016].
- 318 Guerriero, L. Bertello, L., Cadozo, N., Berti, M., Grelle, G., Revellino, P. 2017. Unsteady  
319 sediment discharge in earth flows: A case study from the Mount Pizzuto earth flow,  
320 southern Italy. *Geomorphology*, **295**, 260-284.  
321 <https://dx.doi.org/10.1016/j.geomorph.2017.07.011>
- 322 Guerriero, L., Coe, J.A., Revellio, P., Grelle, G., Pinto, F., Guadagno, F. 2016. Influence of  
323 slip-surface geometry on earth-flow deformation, Montaguto earth flow, southern Italy,  
324 *Geomorphology*, **219**, 285-305. <https://dx.doi.org/10.1016/j.geomorph.2014.04.039>
- 325 Gunn, A.D., Chambers, J.E., Uhlemann, S., Wilkinson, P.B., Meldrum, P.I., Dijkstra, T.D.,  
326 Haslam, E., Kirkham, M., Wragg, J., Holyoake, S., Hughes, P.N, Hen-Jones, R. and  
327 Glendinning, S. 2015. Moisture monitoring in clay embankments using electrical  
328 resistivity tomography. *Construction and Building Materials*, **92**, 82-94,  
329 <http://dx.doi.org/10.1016/j.conbuildmat.2014.06.007>.
- 330 Juerges, A., Pringle, J.K., Jervis, J.R. and Masters, P. (2010). Comparisons of magnetic and  
331 electrical resistivity surveys over simulated clandestine graves in contrasting burial  
332 environments. *Near Surface Geophysics*, **8**, 529-539, [https://dx.doi.org/10.3997/1873-](https://dx.doi.org/10.3997/1873-0604.2010041)  
333 [0604.2010041](https://dx.doi.org/10.3997/1873-0604.2010041).
- 334 Kampke, A. 1999. Focused imaging of electrical resistivity data in archaeological prospecting.  
335 *Journal of Applied Geophysics*, **41**, 215-227, [https://dx.doi.org/10.1016/S0926-](https://dx.doi.org/10.1016/S0926-9851(98)00043-3)  
336 [9851\(98\)00043-3](https://dx.doi.org/10.1016/S0926-9851(98)00043-3).

337 Keary, P., Brooks, M. and Hill, I. 2002. *Introduction to Geophysical Exploration*. 3<sup>rd</sup> edition.  
338 The United Kingdom: Blackwell publishing, **262**.

339 Loke, M.H., Wilkinson, P.B. and Chambers, J.E. 2010. Parallel computing of optimized  
340 arrays for 2-D electrical imaging surveys. *Geophysical Journal International*, **183**, 1302-  
341 1315, <https://dx.doi.org/10.1111/j.1365-246X.2010.04796.x>.

342 Loke, M.H. and Barker, R. D. 1995. Least-square deconvolution of apparent resistivity  
343 pseudosections. *Geophysics*, **60** (6), 1682-1690, <https://dx.doi.org/10.1190/1.1443900>.

344 Loke M.H. and Barker R.D. 1996. Rapid least-squares inversion of apparent resistivity  
345 pseudosections using a quasi-Newton method. *Geophysical Prospection*, **44**, 131–152,  
346 <https://dx.doi.org/10.1111/j.1365-2478.1996.tb00142.x>.

347 Loke M.H., Acworth I. and Dahlin T. 2003. A comparison of smooth and blocky inversion  
348 methods in 2D electrical imaging surveys. *Exploration Geophysics*, **34**, 182–187,  
349 <https://dx.doi.org/10.1071/EG03182>.

350 Loke, M.H. 2015. Tutorial 2-D and 3-D electrical imaging survey. [Available online]:  
351 [www.geotomosoft.com/downloads.php](http://www.geotomosoft.com/downloads.php). Accessed September 2015.

352 Loke, M.H., and Dahlin, T. 2002. A comparison of the Gauss–Newton and quasi-Newton  
353 methods in resistivity imaging inversion. *Journal of Applied Geophysics*, **49**, 149–162,  
354 [https://dx.doi.org/10.1016/S0926-9851\(01\)00106-9](https://dx.doi.org/10.1016/S0926-9851(01)00106-9).

355 Loke, M.H., Chambers, J., Rucker, D.F., Wilkinson, P.B. 2013. Recent developments in the  
356 direct-current geoelectrical imaging method. *Journal of Applied Geophysics*, **95**, 135-156,  
357 <https://dx.doi.org/10.1016/j.jappgeo.2013.02.017>.

- 358 Loke, M.H., Wilkinson, P.B., Chambers, J.E. 2010. Fast computation of optimized electrode  
359 arrays for 2D resistivity surveys. *Computers & Geosciences*, **36**, 1414-1426,  
360 <https://dx.doi.org/10.1016/j.cageo.2010.03.016>.
- 361 Lysdahl, A.K., Bazin, S., Christensen, C., Ahrens, S., Günther, T. and Pfaffhuber, A. 2017.  
362 Comparison between 2D and 3D ERT inversion for engineering site investigation – a case  
363 study from Oslo Harbour. *Near Surface Geophysics*, **15**, 201-209,  
364 <https://dx.doi.org/10.3997/1873-0604.2016052>.
- 365 Long, M., Pfaffhuber, A.A., Bazin, S., Kåsin, K., Gylland, A. and Montaflija, A. 2017.  
366 Glacio-marine clay resistivity as a proxy for remoulded shear strength: correlations and  
367 limitations. *Quarterly Journal of Engineering Geology and Hydrogeology*, **51**, 63-78,  
368 <https://dx.doi.org/10.1144/qjegh2016-136>.
- 369 Cuthbert, M.O., Mackay, R., Tellam, J.H. and Barker, R.D. 2009. The use of electrical  
370 resistivity tomography in deriving local-scale models of recharge through superficial  
371 deposits. *Quarterly Journal of Engineering Geology and Hydrogeology*, **42**, 199-209,  
372 <https://dx.doi.org/10.1144/1470-9236/08-023>.
- 373 Maurer, H., Curtis, A. and Boerner, D.E. 2010. Recent advances in optimized geophysical  
374 survey design. *Geophysics*, **75**, A177-A194, <https://dx.doi.org/10.1190/1.3484194>.
- 375 Nyquist, J.E. and Roth, M.J.S. 2005. Improved 3D pole-dipole resistivity surveys using radial  
376 measurement pairs. *Geophysics Research Letters*, **32**, L21416, 4,  
377 <https://dx.doi.org/10.1029/2005GL024153>.
- 378 Orfanos, C. and Apostolopoulos, G. 2011. 2D-3D resistivity and microgravity measurements  
379 for the detection of an ancient tunnel in the Lavrion area, Greece. *Near Surface*  
380 *Geophysics*, **9**, 449-457, <https://dx.doi.org/10.3997/1873-0604.2011024>.

381 Reynolds, J.M. 2011. *Introduction to Applied and Environmental Geophysics*. 2<sup>nd</sup> ed edition.  
382 John Wiley & Sons, 696.

383 Saad, R., Nawawi, M.N.M., Muztaza, N.M. and Jusoh, Z. 2010. *Testing of resistivity imaging*  
384 *method with different protocols to detect void using miniature model. In; progress of*  
385 *physics research in Malaysia: PERFIK2009*, **1250** (1), 177-180.

386 Soupios, P.M., Georgakopoulos, P, Papadopoulos, N., Saltas, V., Andreadakis, A.,  
387 Vallianatos, F., Sarris, A. and Makris, J.P. 2007. Use of engineering geophysics to  
388 investigate a site for a building foundation. *Journal of Geophysics and Engineering*, **4**, 94–  
389 103, <https://dx.doi.org/10.1088/1742-2132/4/1/011>.

390 Stummer, P., Maurer, H. and Green, A.G. 2004. Experimental design: Electrical resistivity  
391 data sets that provide optimum subsurface information. *Geophysics*, **69**, 120-139,  
392 <https://dx.doi.org/10.1190/1.1649381>.

393 Szalai, S. and Szarka, L. 2008. On the classification of surface geoelectric arrays.  
394 *Geophysical Prospection*, **56**, 159-175, [https://dx.doi.org/10.1111/j.1365-](https://dx.doi.org/10.1111/j.1365-2478.2007.00673.x)  
395 [2478.2007.00673.x](https://dx.doi.org/10.1111/j.1365-2478.2007.00673.x).

396 Tejero-Andrade, A., Cifuentes, G., Chavez, R.E., Lopez-Gonzalez, A.E. and Delgado-  
397 Solorzano, C. 2015. L- and CORNER-arrays for 3D electric resistivity tomography: an  
398 alternative for geophysical surveys in urban zones. *Near Surface Geophysics*, **13**, 355-367,  
399 <https://dx.doi.org/10.3997/1873-0604.2015015>.

400 Wilkinson, P.B., Meldrum, P.I., Chambers, J.E., Kuras, O. and Ogilvy, R.D. 2006. Improved  
401 strategies for the automatic selection of optimized sets of electrical resistivity tomography  
402 measurement configurations. *Geophysical Journal International*, **167**, 1119-1126,  
403 <https://dx.doi.org/10.1111/j.1365-246X.2006.03196.x>.

- 404 Wilkinson, P.B., Loke, M.H., Meldrum, P.I., Chambers, J.E., Kuras, O., Gunn, D.A. and  
405 Ogilvy, R. D. 2012. Practical aspects of applied optimized survey design for electrical  
406 resistivity tomography. *Geophysical Journal International*, **189**, 428-440,  
407 <https://dx.doi.org/10.1111/j.1365-246X.2012.05372.x>.
- 408 Zhu, J., Currens, J.C., Dinger, J.S. and 2011. Challenges of using electrical resistivity method  
409 to locate karst conduits-a field case in the Inner Bluegrass Region, Kentucky. *Journal of*  
410 *Applied Geophysics*, **75** (3), 523–530,  
411 <https://dx.doi.org/doi:10.1016/j.jappgeo.2011.08.009>.
- 412 Zhu, T., Zhou, J. and Wang, H. 2017. Localization and characterization of the Zhandian-  
413 Renhe fault zone in Zibo city, Shandong province, China, using electrical resistivity  
414 tomography (ERT). *Journal of Applied Geophysics*, **136**, 343-352,  
415 <http://dx.doi.org/10.1016/j.jappgeo.2016.11.016>.
- 416
- 417
- 418
- 419
- 420
- 421
- 422
- 423
- 424

425

426

427

428 **Figure captions**

429 **Fig. 1.** (a) plan view and (b & c) side views of the cleared buried wall foundation (brown),  
430 test site gravel infill and top soil fill (marked) within the test pit, with measurements in  
431 metres (adapted from Cassidy 2001).

432

433 **Fig. 2.** Schematic diagram showing the geophysical survey positions on the test site with  
434 (inset) annotated photograph with survey profile locations indicated.

435

436 **Fig. 3.** ERT 2D profile sections in N-S direction using least-square smoothness-constraint  
437 inversion with Wenner, dipole-dipole, pole-dipole, and pole-pole array configurations (see  
438 Fig.2 for location). White boxes indicate cleared wall foundation (solid line) and surrounding  
439 test site (dotted line) positions respectively. Pole-dipole data shown is merged from data  
440 collected in both directions on each profile. Inversion iteration 5 results shown throughout.

441

442 **Fig. 4.** ERT 2D profile sections in E-W direction using least-square smoothness-constraint  
443 inversion with Wenner, dipole-dipole, pole-dipole, and pole-pole array configurations (see  
444 Fig. 2 for location). White boxes indicate cleared wall foundation (solid line) and surrounding  
445 test site (dotted line) positions respectively. Pole-dipole data shown is merged from data  
446 collected in both directions on each profile. Inversion iteration 5 results shown throughout.

447

448 **Fig. 5.** ERT 2D profile sections in N-S direction using robust inversion with Wenner, dipole-  
449 dipole, pole-dipole, and pole-pole array configurations (see Fig. 2 for location). White boxes  
450 indicate cleared wall foundation (solid line) and surrounding test site (dotted line) positions  
451 respectively. Pole-dipole data shown is merged from data collected in both directions on each  
452 profile. Inversion iteration 5 results shown throughout.

453

454 **Fig. 6.** ERT 2D profile sections in E-W direction using robust inversion with Wenner, dipole-  
455 dipole, pole-dipole, and pole-pole array configurations (see Fig. 2 for location). White boxes  
456 indicate cleared wall foundation (solid line) and surrounding test site (dotted line) positions  
457 respectively. Pole-dipole data shown was merged from data collected in both directions on  
458 each profile. Inversion iteration 5 results shown throughout.

459

460

461 **Table 1.** Summary statistics of each ERT profile, array type, data points collected/inverted and depth 'n' levels.  
 462 Fig.2 for profile locations.

| <b>ERT Profile</b> | <b>Array</b>  | <b>No. of collected data points</b> | <b>No. of corrected data points</b> | <b>Data 'n' levels</b> |
|--------------------|---------------|-------------------------------------|-------------------------------------|------------------------|
| <b>NS1</b>         | Wenner        | 600                                 | 7                                   | 15                     |
|                    | Dipole-dipole | 873                                 | 0                                   | 18                     |
|                    | Pole-dipole   | 909                                 | 1                                   | 18                     |
|                    | Pole-pole     | 455                                 | 1                                   | 13                     |
| <b>NS 2</b>        | Wenner        | 600                                 | 1                                   | 15                     |
|                    | Dipole-dipole | 873                                 | 0                                   | 18                     |
|                    | Pole-dipole   | 909                                 | 0                                   | 18                     |
|                    | Pole-pole     | 455                                 | 1                                   | 13                     |
| <b>NS 3</b>        | Wenner        | 600                                 | 20                                  | 15                     |
|                    | Dipole-dipole | 873                                 | 72                                  | 18                     |
|                    | Pole-dipole   | 909                                 | 0                                   | 18                     |
|                    | Pole-pole     | 455                                 | 6                                   | 13                     |
| <b>EW 1</b>        | Wenner        | 600                                 | 0                                   | 15                     |
|                    | Dipole-dipole | 873                                 | 0                                   | 18                     |
|                    | Pole-dipole   | 909                                 | 0                                   | 18                     |
|                    | Pole-pole     | 455                                 | 3                                   | 13                     |
| <b>EW 2</b>        | Wenner        | 600                                 | 2                                   | 15                     |
|                    | Dipole-dipole | 873                                 | 13                                  | 18                     |
|                    | Pole-dipole   | 909                                 | 1                                   | 18                     |
|                    | Pole-pole     | 455                                 | 1                                   | 13                     |
| <b>EW 3</b>        | Wenner        | 600                                 | 0                                   | 15                     |
|                    | Dipole-dipole | 873                                 | 1                                   | 18                     |
|                    | Pole-dipole   | 909                                 | 1                                   | 18                     |
|                    | Pole-pole     | 455                                 | 2                                   | 13                     |

463

464

465



466 **Table 2.** ERT 2D profiles (both least-squares and robust inversions) were qualitatively assessed based on the  
 467 accuracy of the cleared wall foundation position and being successfully imaged. Images were ranked **Good** for  
 468 when the model achieved this, **Moderate** for when the model only achieved one and ranked **Poor** when the  
 469 model did not achieve any parameters. Model RMS inversion percentages also included.  
 470

| 2D Profile number<br>(see Fig.2) and<br>array type | Least-square<br>Inverted model, ,<br>RMS % error<br>misfit | Cleared wall<br>foundation<br>well defined | Robust<br>Inverted<br>model, RMS %<br>error misfit | Cleared wall<br>foundation well<br>defined |
|--|--|--|--|--|
| NS1, Wenner  | 5.0  | Good                                       | 2.8  | Moderate                                   |
| NS1, Dipole-dipole                                 | 5.0  | Good                                       | 2.7  | Moderate                                   |
| NS1, Pole-dipole                                   | 4.1  | Poor                                       | 2.8  | Poor                                       |
| NS1, Pole-pole                                     | 9.3  | Poor                                       | 5.5  | Poor                                       |
| NS2, Wenner  | 4.4  | Moderate                                   | 2.2  | Poor                                       |
| NS2, Dipole-dipole                                 | 5.0  | Moderate                                   | 3.4  | Poor                                       |
| NS2, Pole-dipole                                   | 8.8  | Poor                                       | 4.1  | Poor                                       |
| NS2, Pole-pole                                     | 9.2  | Poor                                       | 4.4  | Poor                                       |
| NS3, Wenner  | 9.4  | N/A (off axis)                             | 4.8  | N/A (off axis)                             |
| NS3, Dipole-dipole                                 | 10.3   | N/A (off axis)                             | 5.2  | N/A (off axis)                             |
| NS3, Pole-dipole                                   | 5.3  | N/A (off axis)                             | 3.4  | N/A (off axis)                             |
| NS3, Pole-pole                                     | 14.9*  | N/A (off axis)                             | 7.1  | N/A (off axis)                             |
| EW1, Wenner  | 5.0  | Good                                       | 3.1  | Moderate                                   |
| EW1, Dipole-dipole                                 | 6.4  | Good                                       | 4.6  | Moderate                                   |
| EW1, Pole-dipole                                   | 6.8  | Moderate                                   | 4.4  | Poor                                       |
| EW1, Pole-pole                                     | 12.7*  | Poor                                       | 7.6*   | Poor                                       |
| EW2, Wenner  | 3.4  | Good                                       | 2.0  | Moderate                                   |
| EW2, Dipole-dipole                                 | 10.1   | Good                                       | 5.0  | Moderate                                   |
| EW2, Pole-dipole                                   | 3.4  | Moderate                                   | 2.0  | Moderate                                   |
| EW2, Pole-pole                                     | 12.0*  | Poor                                       | 5.7  | Poor                                       |
| EW3, Wenner  | 1.8  | N/A (off axis)                             | 2.5  | N/A (off axis)                             |
| EW3, Dipole-dipole                                 | 2.8  | N/A (off axis)                             | 1.7  | N/A (off axis)                             |
| EW3, Pole-dipole                                   | 2.4  | N/A (off axis)                             | 1.5  | N/A (off axis)                             |
| EW3, Pole-pole                                     | 13.9*  | N/A (off axis)                             | 6.3  | N/A (off axis)                             |

471  
 472 \* indicated relatively high model errors.  
 473

## LIST OF FIGURES

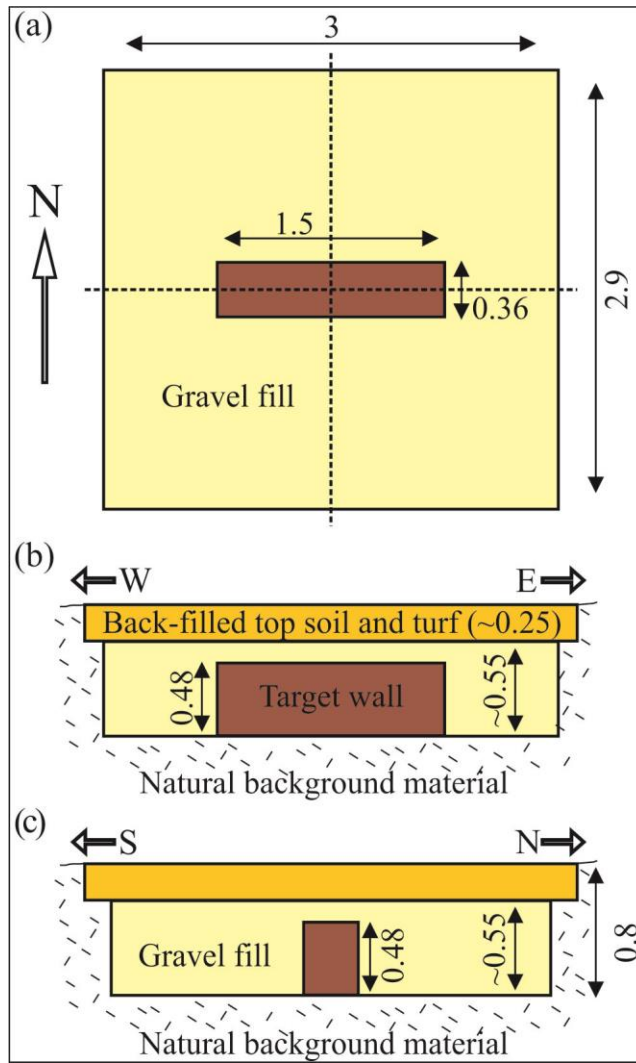


FIGURE 1

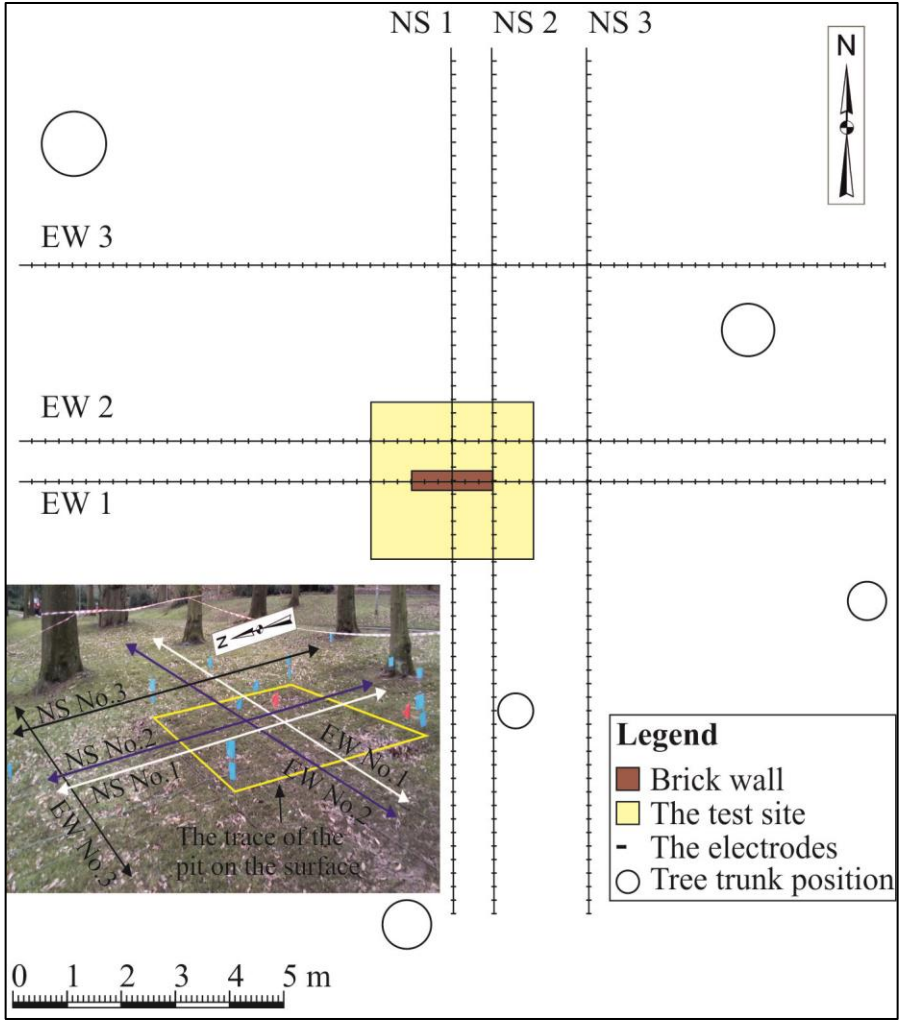


FIGURE 2

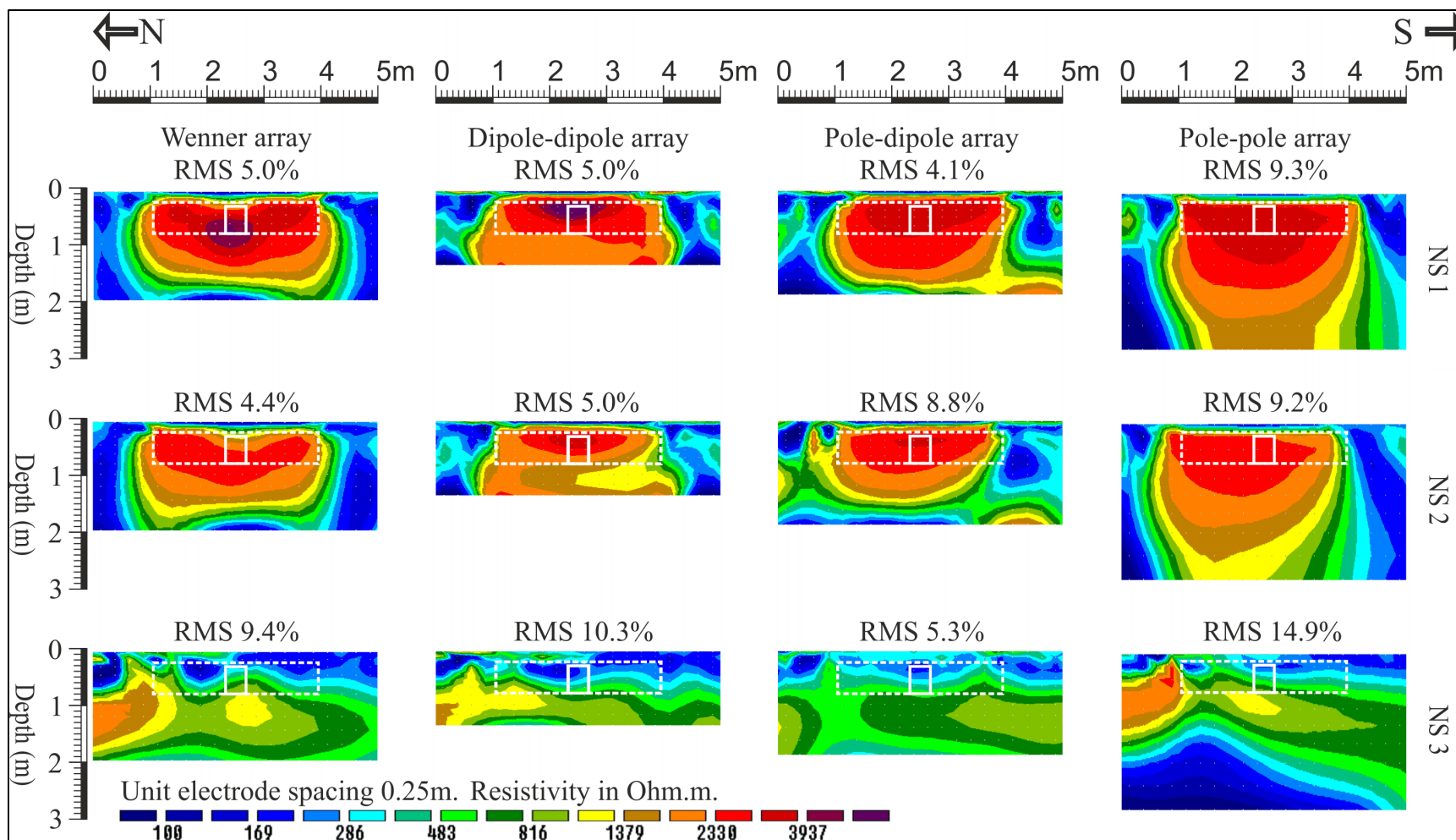


FIGURE 3

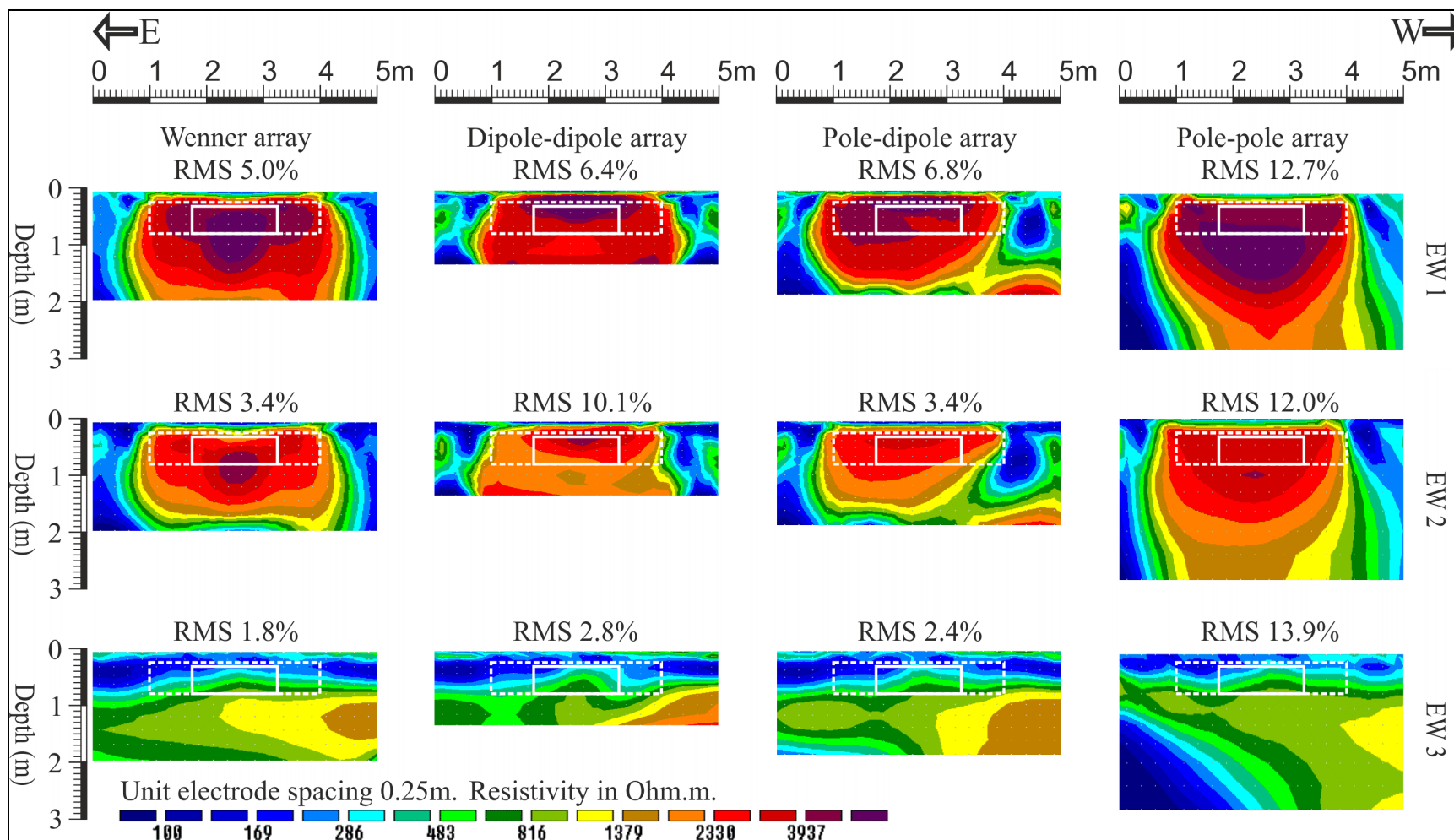


FIGURE 4

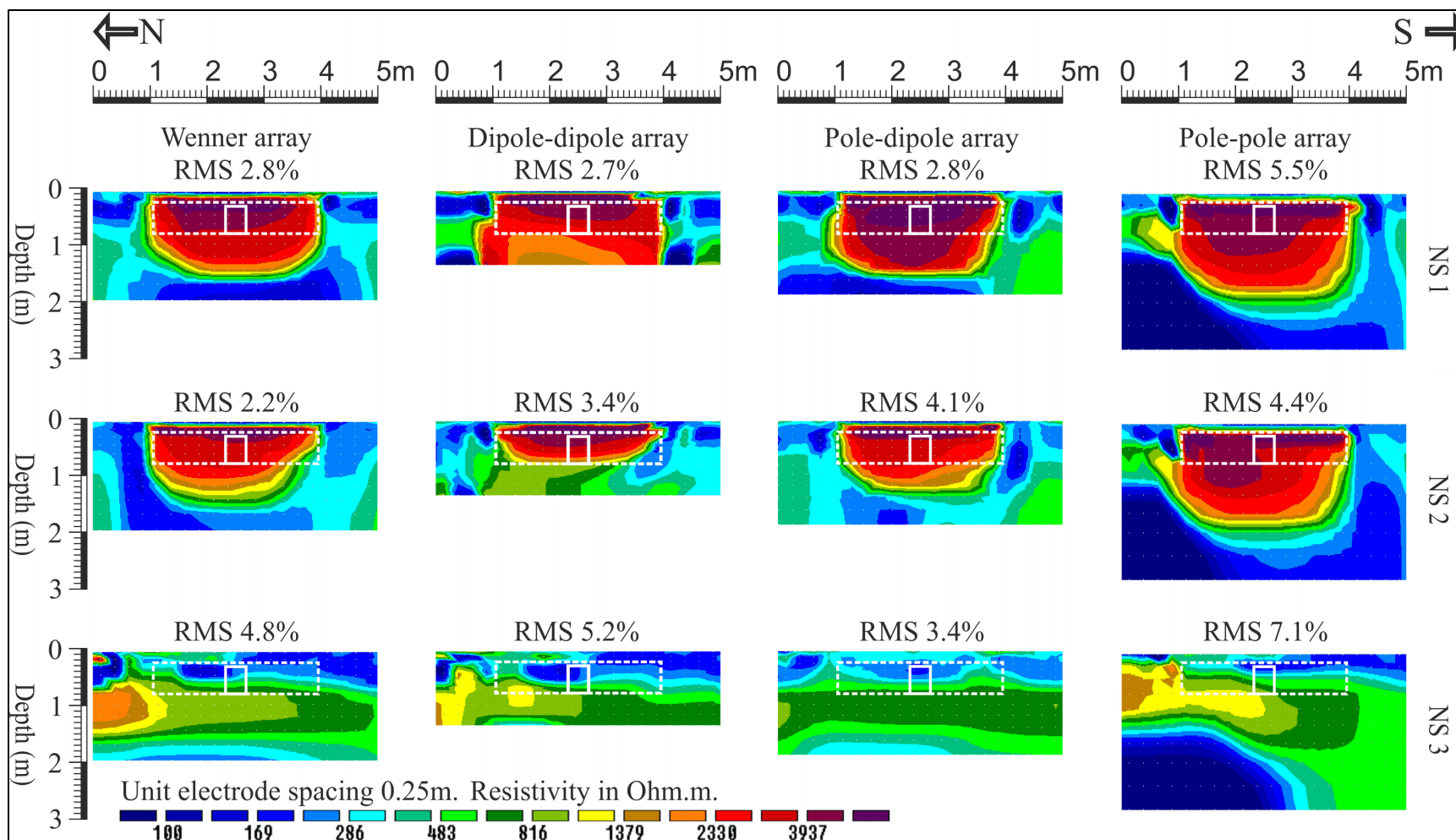


FIGURE 5

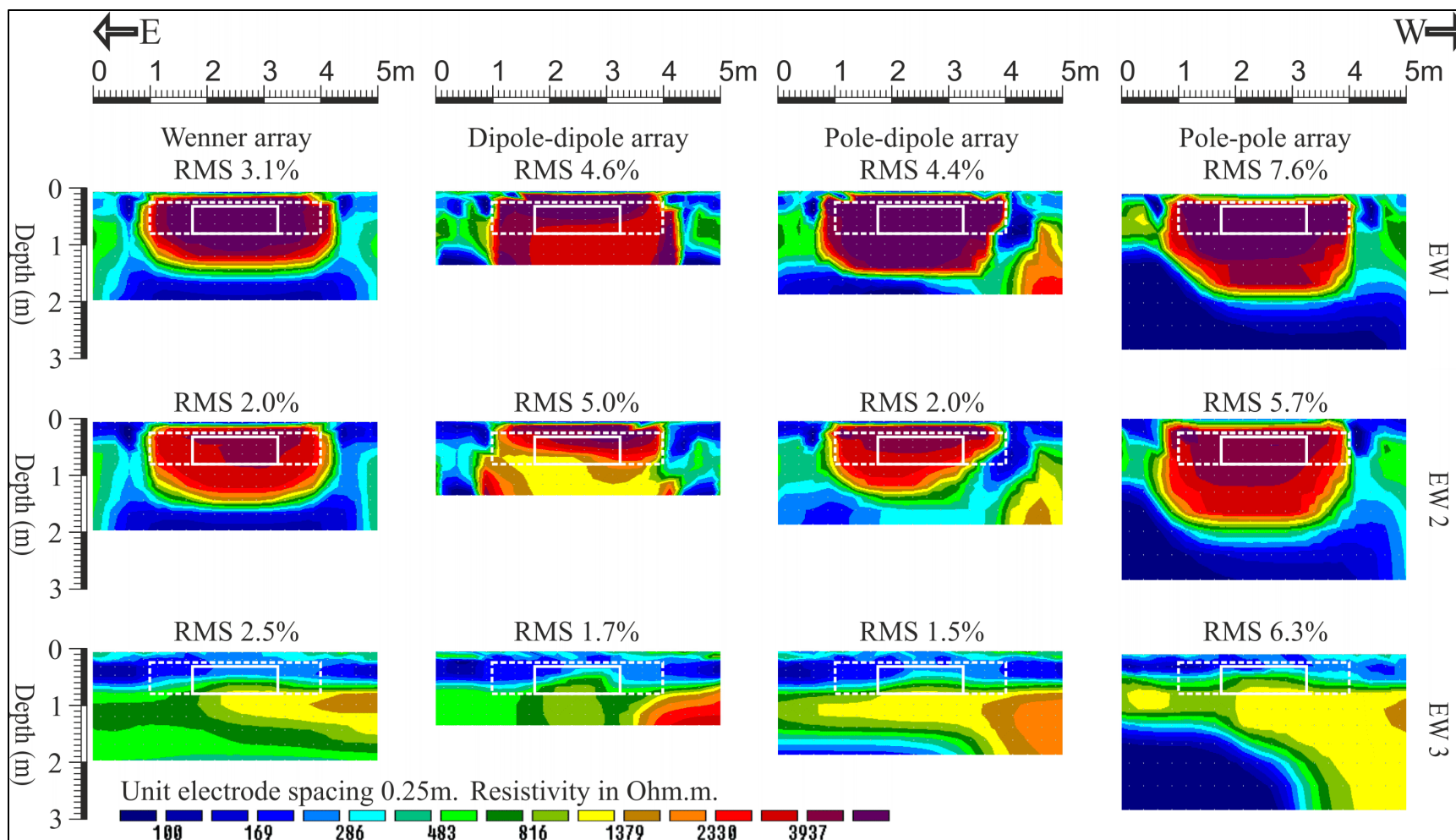


FIGURE 6